Digital architecture to realize programmable central pattern generators producing multiple gaits

Matteo Lodi*, Andrey Shilnikov†, Marco Storace*
*DITEN, University of Genoa, Via Opera Pia 11a, I-16145 Genova, Italy. E-mail: marco.storace@unige.it
†Neuroscience Institute, Georgia State University, 100 Piedmont Ave, Atlanta GA 30303, USA. E-mail: ashilnikov@gsu.edu

***Abstract*—We propose and discuss a digital architecture suitable for hardware implementation of multifunctional neural networks to regulate several gaits for quadruped locomotion. These circuits have a far-reaching application for various bio-inspired robotics and synthetic prosthetics. The circuit is tested by implementing an 8-cell network proposed and analyzed here for the first time, whose robustness is checked with respect to parameter mismatching.**

I. Introduction

Animal legged locomotion is governed by complex dynamics. In order to let the animal move in an efficient and stable way over varied and uncertain terrains, it requires an accurate control for limbs that is agilely responsive and adaptive to sensorimotor errors to avoid falls and collisions in habitual conditions [1]. The locomotion action is tightly coupled with various bio-mechanical (musculoskeletal structure) and neural (control action) factors. Therefore, being inspired by Nature, one has to re-recreate/re-engineer locomotion systems that combine animal morphology and control by neural mechanisms. Neural circuits known as Central Pattern Generators (CPGs), being small neural networks usually located along the spinal column in vertebrates, provide an *open-loop* control to stably generate various rhythmic patterns corresponding to different gaits. Furthermore, locomotion control involves two mechanisms of *closed-loop* control, acting at different timescales [2]. The first one is a sensorimotor control implemented through (spinal) reflexes with fast response times (in the order of few milliseconds), which allow for reacting to unexpected events, such as unseen or badly estimated obstacles causing a sudden lost of balance. The second one is a predictive planning requiring longer processing (in the order of seconds) of sensory stimuli in higher brain centers; this kind of control sets the rhythm generated by the CPG.

In [3] a method has been proposed that allows for designing the synaptic connections in order to obtain different gaits with variations of a control parameter α, representing the neuromodulation induced on the CPG by the higher brain centers drive [4], [5]. In particular, the α parameter models the action of the brain-mediated slower closed-loop control in a synthetic, biologically-inspired CPG composed of macro-models (*cells*) of several subgroups of neurons functioning synchronously. In [6] a reduced model of the reactive sensorimotor-feedback-mediated control for similar CPG circuits was proposed. What should the next step be? We think the digital implementations for rhythm-generating circuits have far-reaching applications for bio-inspired robotics [2], [7] and rehabilitation [8], that require the hardware and software development of these rhythm-generating circuits. This should let one to implement different CPG architectures, and various models of cells and synapses, whose properties (e.g., synaptic weights) vary depending on the control parameter α.

In the last decades, many neuromorphic architectures have been proposed to implement neural networks mimicking specific neural functions [9]–[13], including CPGs [14], [15]. They are often based on "integrate and fire" neuronal models with limited options. On the other hand, small and hence specialized neural networks such as CPGs typically require biophysically plausible and accurate models for their cells. For instance, CPGs are known to demonstrate the so-called post-inhibitory rebound of the cell membrane voltage, which allows reciprocally inhibitory cells to generate self-sustained oscillations in anti-phase [16].

In this paper, we discuss an easily programmable digital architecture, which enables the implementation of a range of synthetic, minimal CPGs that can generate a set of different prescribed rhythms. The key feature of this architecture is its easy on-line reprogramming, which, as described above, allows for embedding neuromodulation in the CPG (through the external drive α) and switching continuously and reliably among different gaits as α is changed. To the best of the authors' knowledge, the only circuit with similar features [17] does not allow for implementing complex cell models and is not portable on different digital circuits, unlike the architecture proposed here. The digital architecture is based on a main board that connects together Processing Units (PU) modeling cells of the CPG. The parameters of individual cells and their connectivity can be changed at run-time through the USB connection. To test the functionality of this circuit, we implement and analyze an 8-cell CPG producing four gaits. Unlike the CPG considered in [3], this 8-cell CPG is designed using a distinct network topology allowing for more biologically-plausible responses of the cells controlling the flexors. In addition, we test the robustness of the gaits produced by the CPG under consideration.

II. Architecture of the CPG circuit

The i-th cell of the CPG is described by a set of ODEs:

$$\dot{\mathbf{z}}_i = \begin{bmatrix} \dot{V}_i \\ \dot{\mathbf{x}}_i \end{bmatrix} = \begin{bmatrix} f_i(\mathbf{z}_i, \alpha, I_{syn}^{(i)}(\alpha)) \\ \mathbf{p}_i(\mathbf{z}_i) \end{bmatrix}, \tag{1}$$

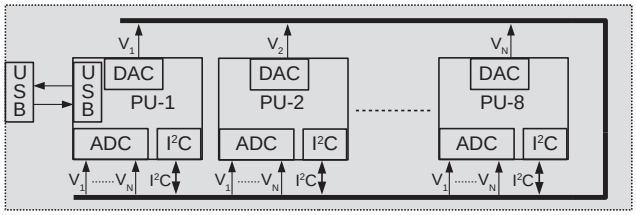

Fig. 1. Scheme of the digital CPG circuit. The circuit contains N PUs (corresponding to the N CPG cells), each one of which computes the time evolution of $\mathbf{z}_i$. The PUs share CPG parameters through I^{2}C bus.

here $\mathbf{z}_i = \left[V_i\ \mathbf{x}_i^T\right]^T$ (whose physical dimensions depend on the chosen cell model) is a state vector with V_i being the membrane potential directly acting on the legs and on the synapses, $\mathbf{x}_i$ is a vector of auxiliary state variables, $[f_i\ \mathbf{p}_i^T]^T$ is the vector field determining the cell dynamics, and α is the parameter representing the brain control. The term $I_{syn}^{(i)}(\alpha)$, representing the incoming synaptic current, which is due to chemical (inhibitory and excitatory) or electrical synapses, is given by

$$I_{syn}^{(i)} = \sum_{j=0}^{N-1} g_{ij}^{in}(\alpha) h_{in}(V_j)(E_{in} - V_i) + \sum_{j=0}^{N-1} g_{ij}^{ex}(\alpha) h_{ex}(V_j)(E_{ex} - V_i) + \sum_{j=0}^{N-1} g_{ij}^{el}(\alpha)(V_j - V_i) \quad (2)$$

The inhibitory (excitatory) synapse activation h_{in} (h_{ex}) is an algebraic function of the pre-synaptic cell membrane potential V_j and g_{ij}^{in} (g_{ij}^{ex}) is the strength of the inhibitory (excitatory) chemical synapse between cells i and j. Similarly, g_{ij}^{el} is the strength of the electrical synapse between cells i and j. All the synaptic strengths are non-negative numbers.

To implement this model into the digital circuit, we adopt the architecture shown in Fig. 1; it allows building a CPG composed of up to N cells. The circuit is composed of N Processing Units (PUs), corresponding to the N CPG cells. Each unit contains at least one of each of the following elements: Analog to Digital Converter (ADC), Digital to Analog Converter (DAC), RAM, Direct Memory Access (DMA), timers and Central Processing Unit (CPU) with floating-point Arithmetic-Logic Unit (ALU). The i-th CPU computes the time progression of the state vector $\mathbf{z}_i$, while the DAC converts the cell membrane potential V_i into an analog signal. Each processing unit receives the analog membrane potentials V_j ($j = 1, \ldots, N$) of all cells and converts them into digital signals through the ADC. Every processing unit is assigned a unique address (between 1 and N) that is shared on the I^2C bus; these identifiers are used to configure parameters of the cells. In particular, a PC sends the control α-parameter value through USB port to processing unit 1, which next configures itself and passes the α value to the other cells through I^2C bus. The use of the low-speed (serial) protocol I^2C bus justifies the need of ADCs and DACs. A faster (parallel) protocol could allow the use of digital signals only, thus avoiding the use of converters, at the cost of a reduced scalability to larger networks or to more complex cell models. Both USB and I^2C communications are managed by interrupt. Figure 2 shows a

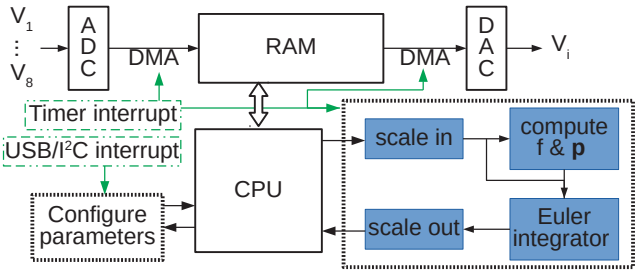

Fig. 2. Block-scheme of the i-th processing unit. The main CPU task is to compute the state evolution through the forward Euler's method. The communication with the PC and the other PUs is managed by interrupts.

more detailed block-scheme of the i-th processing unit, whose function is to compute the time evolution of the state vector $\mathbf{z}_i$. A timer interrupt is emitted every Δt seconds. When the k-th timer interrupt occurs, the DMA moves the sampled membrane potentials $V_j(k\Delta t)$ of the other cells from ADC to RAM, and then the CPU computes the next state sample as follows:

$$\mathbf{z}_i((k+1)\Delta t) = \mathbf{z}_i(k\Delta t) + \Delta t\ \dot{\mathbf{z}}_i(k\Delta t) \quad (3)$$

by integrating Eqs. (1) using the Euler method. The computed $\mathbf{z}_i((k+1)\Delta t)$ value is stored in RAM and then is moved to DAC by the DMA when the $(k+1)$-th timer interrupt is emitted. Blocks *scale in* and *scale out* depend on the chosen cell model and provide a linear scaling between ADC and DAC range to the range of cell membrane potential.

III. Case Study: 8-cell CPG for Mouse Locomotion

As a case study, we consider the CPG for mouse locomotion shown in Fig. 3; its circuitry is deduced by applying the synthesis method described in [3] to a bio-inspired CPG [18]. The CPG behavior is controlled by the parameter $\alpha \in [0, 1]$, which determines both the speed and the gait produced by the CPG. This CPG can generate the frequency and rhythmic patterns matching walk, trot, gallop and bound gaits of mice. The CPG includes four flexor (1-4) and four extensor (5-8, labeled with E) cells that can be grouped into four flexor-extensor pairs,

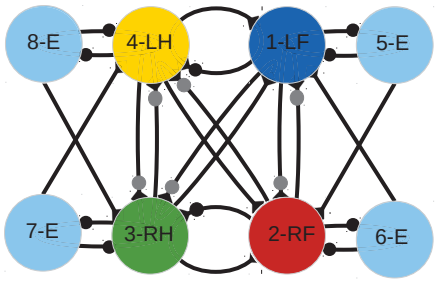

Fig. 3. The wiring circuitry of the CPG with mixed, excitatory and inhibitory, synapses between its constituent cells.

each one driving a limb (L=left, R=right, H=hind, F=fore). The cells shown in Fig. 3 are coupled by chemical inhibitory (lines with solid dots) and excitatory (lines with triangle) synapses. Lines with the gray dots indicate inhibitory synapses whose strengths change with α, as described in the Appendix.

The cells are described by the same model proposed in [18] (and not reported here for conciseness), whereas the synaptic models are described using the fast threshold modulation (FTM) paradigm [19] as follows:

$$h_{in}(V_j) = h_{ex}(V_j) = \frac{1}{1 + e^{-\nu(V_j - \theta)}}; \quad (4)$$

where ν and θ determine the shape of the sigmoidal synaptic activation function. All parameters are given in the Appendix.

In what follows we argue that our CPG model has certain advantages to maintain and regulate quadruped locomotion as:

- it contains fewer cells than the CPGs examined in [5], [18] while generates the same gaits;
- compared to the CPGs proposed in [3], [20], it contains the same number of cells but is more efficient and functional, as the α-drive acts on the left (1 and 4) and right (2-3) flexors uniformly;
- while it contains more cells than the CPGs proposed in [6], [21], it is more biologically plausible because does not rely on delayed synapses, which lets the brain drive influence all the flexors in homogeneous way.

A. Circuit implementation

Figure 4 shows the digital circuit implementation of the 8-cell CPG. The CPG circuit is implemented on a (copper) main board equipped with eight STM32F415 micro-controllers (on the smaller green boards realizing the PUs). Each one (running at 168 MHz) contains three multiplexed ADCs (reading up to 16 analog channels with a maximum rate of 2.4×10^6 samples per second), two 12-bit DACs, DMA, 32-bit timers and a floating point unit. Two AD8608 operational amplifiers, between DACs and ADCs, in buffer configuration are used to uncouple the converters. All micro-controllers have a unique address (1 to 8) and share the I^2C bus.

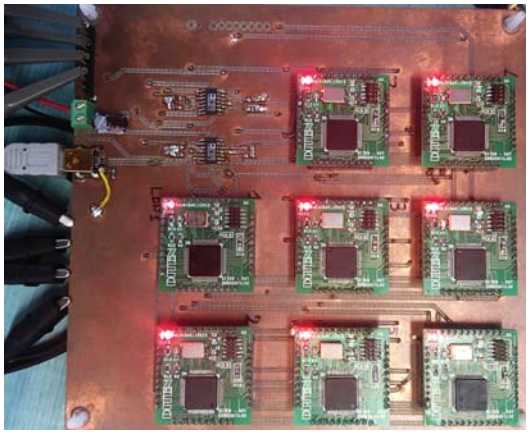

Fig. 4. Implemented 8-cell digital CPG circuit. The main (copper) board contains 8 PUs (green boards).

IV. Results

First, using the MATLAB-based CEPAGE toolbox [22] we examine how the 8-cell CPG regulates the locomotion of mice. Specifically, we evaluate the frequency f (directly related to the animal speed), the duty-cycle dc (measuring the ratio between stand and swing phases) and the phase differences Δ_{1i} between the first and the i-th cells (corresponding to the synchronization between the limbs) through the computational method proposed in [20]. The asymptotic phase differences Δ_{1i}, the frequency f and duty-cycle dc of each cell, computed for 100 values of α linearly-equally spaced between 0 and 1, are shown in Figs. 5- 6. For $\alpha < 0.2$ (green region) the CPG produces the walk gait with a low frequency ($f < 4$Hz), the phase difference 0.5 between alternating cells 1 and 2, while the phase differences Δ_{13} and Δ_{14} are close to 0.25 and 0.75, respectively. The trot gait is produced when $0.2 < \alpha < 0.9$ (light blue region) with cells 1-2 and 1-4 activating in alternation ($\Delta_{12} = \Delta_{14} \approx 0.5$) at the mid frequency range $[4, 10]$Hz. In the gray region with $0.9 < \alpha < 0.93$ the CPG becomes bi-stable due to a supercritical pitchfork bifurcation; moreover the pattern generated in this region does not correspond to any natural gaits. When α is increased to $[0.93, 0.95]$ (pink region), the CPG produces the rotatory gallop gait with fore flexors activating nearly in-phase $\Delta_{12} < 0.1$ (or $\Delta_{12} > 0.9$) and in anti-phase with the hind cells as $\Delta_{14} \approx 0.5$. This region also presents bi-stability with two steady states corresponding to the same pattern but with reverse activation order between the cells. Finally, when $\alpha > 0.95$ (yellow region), the CPG, having become mono-stable due to another supercritical pitchfork bifurcation at $\alpha = 0.95$, produces the bound gait at a higher

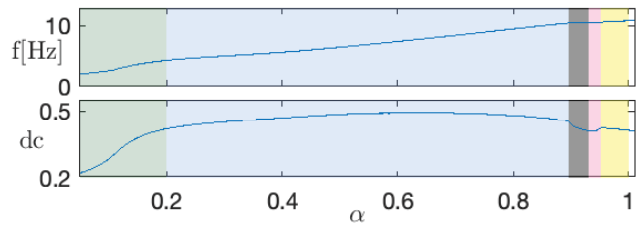

Fig. 5. Frequency f (upper panel) and duty cycle dc (lower panel) plotted against the drive α for four gaits produced by the CPG. Color regions: combinations of f and dc corresponding to walk (green), trot (light blue), gallop (pink), bound (yellow) and no biological gait (gray).

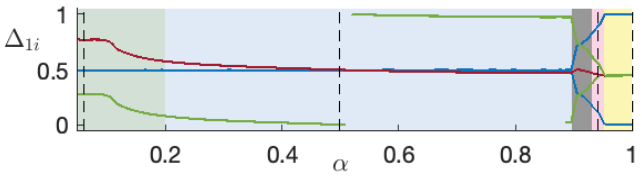

Fig. 6. Asymptotic phase differences Δ_{1i}, with $i = 2$ (blue), $i = 3$ (red) and $i = 4$ (green). Branching points at $\alpha = 0.9$ and $\alpha = 0.95$ are due to supercritical pitchfork bifurcations. Vertical dashed lines: α-vales used in the hardware tests. Color regions: Δ_{1i} corresponding to walk (green), trot (light blue), gallop (pink), bound (yellow) and no biological gait (gray).

frequency ($f > 10Hz$) so that cells 1-2 and 3-4 activate together ($\Delta_{12} = 0$), whereas the phase difference between alternating front and hind cells is 0.5. We remark that the obtained results are coherent with the biological data in [23].

To check the robustness of the obtained CPG against variations in the synaptic strengths, we added a random mismatch to the non-zero entries of the synaptic matrices: $g_{ij}^{xx} = g_{ij}^{xx}(1 + N(0, \sigma))$, with $xx \in \{in, ex\}$. Among all the CPG parameters, we check the robustness against variations in the synaptic strengths, as the topology is chosen a priori as a part of the design procedure while its dependence on the choice of models is investigated in [21]. The standard deviation σ was set to the following values: 1%, 2.5% and 5%, respectively. We analyzed 100 values of α and 100 trials for each value of α. Mean and standard deviation of the obtained results were computed. The corresponding asymptotic phase differences Δ_{1i} are shown in Fig. 7 from the upper to lower panel, respectively.

The found mean values agree very well with the results illustrated in Fig. 6. One can see that Δ_{14} (green line) is the most resilient compared the other asymptotic phase-differences for any α value. On the contrary, Δ_{12} (blue line) is robust (0.5) only when $\alpha < 0.8$; this suggests that the fore-hind connections in this CPG exhibit a greater stability than the left-right ones. As a consequence, the walk and trot gaits are the most robust and efficient gaits, which correspond to the left-right alternation with $\Delta_{12} = 0.5$.

We measured the flexor cells membrane potentials through a RIGOL DS1104 oscilloscope for 51 α-values, equally spaced in the interval $[0, 1]$. The bifurcation diagram of the steady-state phase differences Δ_{1i} is indistinguishable from the one shown in Fig. 6 and therefore is not reported here. The measured $V_i(t)$ obtained for the four values of α corresponding to the vertical dashed lines in Fig. 6 are shown in Fig. 8. From top to bottom, the circuit generates walk ($\alpha = 0.05$), trot ($\alpha = 0.5$), gallop ($\alpha = 0.94$) and bound ($\alpha = 1$).

V. Concluding Remarks

We proposed a circuit architecture specifically tailored to CPGs implementations targeting robotics and rehabilitation/prosthetics applications. Its main advantage is its high flexibility, as it lets various models of cells and synapses be tested by the software tool CEPAGE [22] and chosen to compose rhythm-generating neural networks. Both cell and synapse parameters can be easily and dynamically changed on-line by acting on α, thus making it possible to emulate various gaits through a brain-mediated closed-loop control without re-programming the PUs. With respect to single-PU architectures [24], the proposed distributed architecture exploits parallelism and can also implement biologically plausible and hence computationally expensive models, including the Hodgkin-Huxley types.

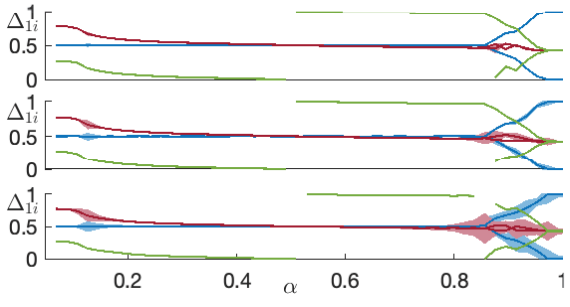

Fig. 7. Asymptotic phase differences Δ_{1i}, with $i = 2$ (blue), $i = 3$ (red) and $i = 4$ (green) for standard deviation of the parameter mismatch set to 1% (top), 2.5% (middle) and 5% (bottom). Dark solid lines: mean values. Shaded strips indicate the mean $\pm$ standard deviation.

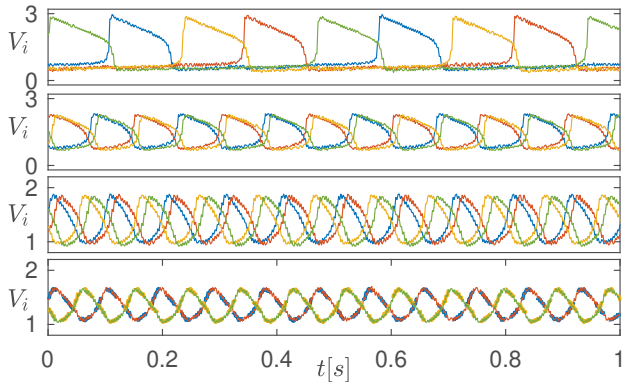

Fig. 8. Membrane voltages $V_i(t)$ generated by the circuit CPG for the flexor cells for α-values corresponding to the vertical dashed lines in Fig. 6 (color code as for the cells in Fig. 3). From top to bottom: walk ($\alpha = 0.05$), trot ($\alpha = 0.5$), gallop ($\alpha = 0.94$) and bound ($\alpha = 1$).

Appendix

The synaptic weights are listed in Table I. Those depending on α are shown in Fig. 9.

TABLE I
Synaptic parameters of the CPG.

Connections	value [nS]	Connections	value [nS]
g_{12}^{ex}, g_{21}^{ex}, g_{34}^{ex}, g_{43}^{ex}	0.0733	g_{15}^{in}, g_{26}^{in} , g_{37}^{in}, g_{48}^{in}	0.1992
g_{36}^{ex}, g_{45}^{ex}	0.0320	g_{51}^{in}, g_{62}^{in}, g_{73}^{in}, g_{84}^{in}	2.5740
g_{42}^{ex}, g_{31}^{ex}	0.0602	g_{41}^{in}, g_{32}^{in}	0.0437
g_{24}^{ex}, g_{13}^{ex}	0.1957	g_{12}^{in}, g_{21}^{in}, g_{34}^{in}, g_{43}^{in}	$g_1(\alpha)$
g_{18}^{ex}, g_{27}^{ex}	0.4003	g_{42}^{in}, g_{31}^{in}	$g_2(\alpha)$

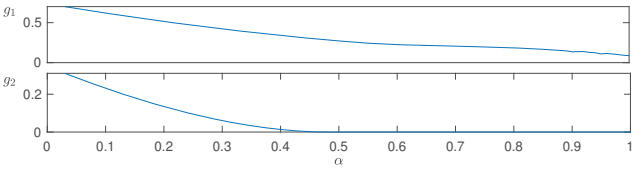

Fig. 9. Functions that describe inhibitory synapse strengths.

The other parameters are set to the following values: $E_{in} = -75$ [mV], $E_{ex} = -10$ [mV], $\theta = -33.5$ [mV], $\nu = 0.2$ [1/mV].

REFERENCES

[1] M. Daley, "Non-steady locomotion," in *Understanding Mammalian Locomotion: Concepts and Applications*, J. Bertram, Ed. John Wiley & Sons, 2016, pp. 277–306.

[2] A. Ijspeert, "Decoding the neural mechanisms underlying locomotion using mathematical models and bioinspired robots: from lamprey to human locomotion," in *Robotics Research*, A. Bicchi and W. Burgard, Eds. Springer, 2018, pp. 177–186.

[3] M. Lodi, A. Shilnikov, and M. Storace, "Design of synthetic central pattern generators producing desired quadruped gaits," *IEEE Transactions on Circuits and Systems I: Regular papers*, vol. 65, no. 3, pp. 1028–1039, 2018.

[4] C. P. Santos and V. Matos, "Gait transition and modulation in a quadruped robot: A brainstem-like modulation approach," *Robotics and Autonomous Systems*, vol. 59, no. 9, pp. 620–634, 2011.

[5] S. M. Danner, S. D. Wilshin, N. A. Shevtsova, and I. A. Rybak, "Central control of interlimb coordination and speed-dependent gait expression in quadrupeds," *The Journal of physiology*, vol. 594, no. 23, pp. 6947–6967, 2016.

[6] M. Lodi, A. Shilnikov, and M. Storace, "Design of minimal synthetic circuits with sensory feedback for quadruped locomotion," in *2018 IEEE International Symposium on Circuits and Systems (ISCAS)*, May 2018, pp. 1–5.

[7] Y. Hu, J. Liang, and T. Wang, "Parameter synthesis of coupled nonlinear oscillators for CPG-based robotic locomotion," *IEEE Transactions on Industrial Electronics*, vol. 61, no. 11, pp. 6183–6191, 2014.

[8] J. A. Bamford, R. M. Lebel, K. Parseyan, and V. K. Mushahwar, "The fabrication, implantation, and stability of intraspinal microwire arrays in the spinal cord of cat and rat," *IEEE Transactions on Neural Systems and Rehabilitation Engineering*, vol. 25, no. 3, pp. 287–296, 2017.

[9] C. Mead, "Neuromorphic electronic systems," *Proceedings of the IEEE*, vol. 78, no. 10, pp. 1629–1636, 1990.

[10] G. Indiveri, B. Linares-Barranco, T. J. Hamilton, A. Van Schaik, R. Etienne-Cummings, T. Delbruck, S.-C. Liu, P. Dudek, P. Häfliger, S. Renaud *et al.*, "Neuromorphic silicon neuron circuits," *Frontiers in neuroscience*, vol. 5, p. 73, 2011.

[11] B. V. Benjamin, P. Gao, E. McQuinn, S. Choudhary, A. R. Chandrasekaran, J.-M. Bussat, R. Alvarez-Icaza, J. V. Arthur, P. A. Merolla, and K. Boahen, "Neurogrid: A mixed-analog-digital multichip system for large-scale neural simulations," *Proceedings of the IEEE*, vol. 102, no. 5, pp. 699–716, 2014.

[12] S. Moradi, N. Qiao, F. Stefanini, and G. Indiveri, "A scalable multicore architecture with heterogeneous memory structures for dynamic neuromorphic asynchronous processors (dynaps)," *IEEE Transactions on Biomedical Circuits and Systems*, vol. 12, no. 1, pp. 106–122, 2018.

[13] H. Soleimani and E. Drakakis, "An efficient and reconfigurable synchronous neuron model," *IEEE Transactions on Circuits and Systems II: Express Briefs*, vol. 65, no. 1, pp. 91–95, 2018.

[14] I. Köymen and E. M. Drakakis, "Current-input current-output analog half center oscillator and central pattern generator circuits with memristors," *International Journal of Circuit Theory and Applications*, vol. 46, no. 7, pp. 1294–1310, 2018.

[15] K. Nakada, T. Asai, and Y. Amemiya, "An analog CMOS central pattern generator for interlimb coordination in quadruped locomotion," *IEEE Transactions on Neural Networks*, vol. 14, no. 5, pp. 1356–1365, 2003.

[16] X.-J. Wang and J. Rinzel, "Alternating and synchronous rhythms in reciprocally inhibitory model neurons," *Neural computation*, vol. 4, no. 1, pp. 84–97, 1992.

[17] T. M. Gorton, "Tangible toolkits for reflective systems modeling," Ph.D. dissertation, Massachusetts Institute of Technology, 2003.

[18] S. M. Danner, N. A. Shevtsova, A. Frigon, and I. A. Rybak, "Computational modeling of spinal circuits controlling limb coordination and gaits in quadrupeds," *Elife*, vol. 6, p. e31050, 2017.

[19] D. Somers and N. Kopell, "Rapid synchronization through fast threshold modulation," *Biological cybernetics*, vol. 68, no. 5, pp. 393–407, 1993.

[20] J. Wojcik, J. Schwabedal, R. Clewley, and A. Shilnikov, "Key bifurcations of bursting polyrhythms in 3-cell central pattern generators," *PloS one*, vol. 9, no. 4, p. e92918, 2014.

[21] M. Lodi, A. Shilnikov, and M. Storace, "Design principles for central pattern generators with preset rhythms," *IEEE Transactions on Neural Networks and Learning Systems*, submitted.

[22] ——, "CEPAGE: A toolbox for central pattern generator analysis," in *Circuits and Systems (ISCAS), 2017 IEEE International Symposium on*. IEEE, 2017, pp. 1–4.

[23] C. Bellardita and O. Kiehn, "Phenotypic characterization of speed-associated gait changes in mice reveals modular organization of locomotor networks," *Current Biology*, vol. 25, no. 11, pp. 1426 – 1436, 2015.

[24] L. Li, C. Wang, and G. Xie, "A general CPG network and its implementation on the microcontroller," *Neurocomputing*, vol. 167, pp. 299–305, 2015.